JOURNAL OF MATERIALS SCIENCE: MATERIALS IN MEDICINE, 6 (1995) 249–257

The influences of plasma spraying parameters on the characteristics of hydroxyapatite coatings: a quantitative study

C. Y. YANG
Department of Orthopedics, National Cheng Kung University Medical Center, Tainan, Taiwan

B. C. WANG, E. CHANG
Department of Materials Science and Engineering, National Cheng Kung University, Tainan, Taiwan

J. D. WU
Industrial Technology Research Institute, Hsinchu, Taiwan

All laboratory-made plasma-sprayed hydroxylapatite coatings (HACs) were found to undergo, to different degrees, changes in phase composition, crystallinity, morphology and roughness dependent on plasma spraying parameters (PSPs). The PSPs, which were systematically varied, included the plasma atmosphere, the spraying current and the stand-off distance. Through the determinations of the concentration of impurity phase (CIP) and the index of crystallinity (IOC), the extent of phase purity and the degree of crystallinity of HACs were quantitatively assessed, respectively. Coatings consisting of at least 50% (IOC > 50%) of the original crystalline structure and almostly 95% (CIP < 5%) apatite with barely detectable extra phases were obtained. The microstructure of HACs exhibited great deviations both in morphology from molten to partial molten state and in roughness from coating of high irregularity ($R_a = 14.48\ \mu m$) to a smoother ($R_a = 4.46\ \mu m$) one, dominantly influenced by the spraying atmosphere. As the terms of CIP and IOC are defined and established, the biological responses related to phase purity and crystallinity of HACs can be further evaluated *in vitro* and *in vivo*.

1. Introduction

Applications of bioactive calcium phosphate ceramics as coatings on bioinert metallic substrate to promote fixation of orthopaedic prostheses have received worldwide attention [1–4]. Current laboratory animal studies on plasma-sprayed hydroxyapatite (HA)-coated titanium implants have shown that the thin layer of HA coating (HAC) displays many biological advantages, such as the formation of chemical bonding firmly to bone [5, 6], promotion of normal bone apposed on its surface [7–12], enhancement of tissue ingrowth into the pores of HA-coated metallic implant [13], and protection of surrounding bone against metal-ion release from metallic implants [14, 15]. Moreover, reports of initial clinical human studies on plasma-sprayed HA-coated hip prostheses have revealed encouraging results [16, 17].

Changes in the characteristics of HA material after the plasma spraying process have been proposed [14, 18–25]. In previous studies, undesirable phenomena, including the appearance of impurity phases, reduced crystallinity, deviation of Ca/P stoichiometry and the occurrence of dehydroxylation, were evident. These findings suggest adverse effects on the biological responses of HACs. Therefore, concerns have been focused on the retention of the original characteristics of the HA ceramic. To achieve this, emphases have been given to the coating technique and the properties of the starting HA particles, which were considered to dominantly influence the resulting coating characteristics [23].

More recently, reports have indicated that the phase composition and microstructure of HACs depends on the starting HA particle characteristics [22–25]. High purity in the HAC phase could consequently be obtained [23] and crack-free HAC morphology could be achieved [24]. However, considerations were seldom given to evaluation of the systematic relationships between the coating characteristics and the coating techniques, correspondingly, the plasma spraying parameters (PSPs). We have assumed that PSPs might be an important factor affecting the coating characteristics, and therefore the influence of PSPs on coating characteristics should be subject to detailed investigation.

It has been suggested that the biological responses of HACs *in vivo* were dominantly affected by the phase purity and crystallinity of HACs. However, the influence of both these factors has not yet been quantified. One possible reason is that there were no standard

0957-4530

methods to determine them quantitatively. Thus an acceptable method for quantitative analyses should be established.

In this study, the variation of phase composition, crystallinity and microstructure of HACs with different PSPs were evaluated. The systematically varied PSPs used for the coating process were the plasma atmospheres, the spraying current (SA) and the stand-off distances (SOD). Moreover, through calculation of the concentration of impurity phase (CIP) and the index of crystallinity (IOC), phase purity and crystallinity of the HACs were quantitatively assessed.

2. Materials and methods

2.1. Hydroxyapatite powder (HAP)

Commercial (Amdry 6020, Sulzer Plasma Technik, Inc.) HAP with a near-theoretical stoichiometry (Ca/P = 1.69) [25] was used in the coating process. The HAP had a particle size of 45–125 μm.

2.2. Atmospheric plasma spray

Plates of bioinert Ti–6Al–4V alloy (ASTM F-136) were selected as substrate. Prior to spraying, their surfaces were degreased with dilute acid to remove organic contaminants and grit-blasted with Al_2O_3 to roughen the surface. High purity argon (Ar) at a flow rate of 3.2 l/min was used to carry the HAP at about 20 g/min from a powder feeder to the plasma torch of a plasma spraying system (Plasma Technik, M 1100-C). With the plasma atmospheres (primary plasma Ar gas with hydrogen or helium gas), the spraying current (SA = 400, 500 and 600 A) and the stand-off distances (SOD = 7.5, 15 and 22.5 cm) serving as variables, a total of 54 PSPs were employed (Table I). For Group I PSPs in Table I, hydrogen (H_2) gas with rates 2, 6 and 10 l/min was used as the secondary plasma gas; for Group II PSPs in Table I, helium (He) gas with flow rates 30, 50 and 100 l/min served as the secondary plasma gas. An $X-Y$ robot arm was used to move the plasma gun at constant speed across the substrates so that a uniform coating could be deposited. After six cycles of robot arm movement, the coating thickness depended on the PSPs. During spraying, the substrate was kept at low temperature by compressed air cooling in order to prevent overheating.

2.3. Characteristics of HAP and HACs

2.3.1. Concentration of impurity phase (CIP)

The phases present in the HAP and HACs were identified by X-ray diffractometer (XRD, Rigaku D/MAX III. V) with a scan speed of 4°/min between 20° and 60° (2θ angle), using CuK_α radiation (30 kV; 20 mA). Samples used had equal areas of 1 cm^2. To judge the extent of phase purity in each HAC, the concentration of impurity phases (CIP) was estimated based on the assumption that impurity phases in the amorphous component of HAC (Fig. 1) could be neglected:

$$\mathrm{CIP} = \frac{I_{\mathrm{im}}}{I_0} \times 100\%$$

where I_{im} is the sum of the main peak intensity of all impurity phases in each HAC and I_0 is the main peak intensity of the HA phase in the HAP. The main peak intensity (area of the peak) of phases was integrated by computer using the XRD patterns. The main reflection peaks of HA and possible impurity phases marked by the 2θ angle in the XRD pattern are listed in Table II. Coatings with higher CIP value correspond to poorer phase purity.

2.3.2. Index of crystallinity (IOC)

To evaluate the degree of coating crystallinity, the relative crystallinity index (IOC) was introduced and

TABLE I Plasma spraying parameters (PSPs) employed for manufacturing HACs

	Parameters to be varied
Group I	Secondary plasma gas: hydrogen (H_2) Flow rate of secondary plasma gas (l/min): 2, 6, 10 Spraying current (A): 400, 500, 600 Stand-off distance (cm): 7.5, 15, 22.5
Group II	Secondary plasma gas: helium (He) Flow rate of secondary plasma gas (l/min): 30, 50, 100 Spraying current (A): 400, 500, 600 Stand-off distance (cm): 7.5, 15, 22.5
Fixed parameters	Primary plasma gas/flow rate (l/min): Argon/41 Carrier gas/flow rate (l/min): Argon/3.2 Powder feed rate (g/min): 20 Surface speed (cm/min): 7500 Transverse speed (cm/min): 60

TABLE II The main reflection peaks indicated by the 2θ angle of HA and impurity phases

Phases	2θ	JCPDS number[a]
$Ca_{10}(PO_4)_6(OH)_2$ (HA)	31.8	9–432
$Ca_4P_2O_9$ (TP)	29.7	25–1137
α-$Ca_3(PO_4)_2$ (α-TCP)	30.7	9–348
β-$Ca_3(PO_4)_2$ (β-TCP)	31.0	9–169
CaO	37.2	4–777

[a] JCPDS: Joint Committee on Powder Diffraction Standards.

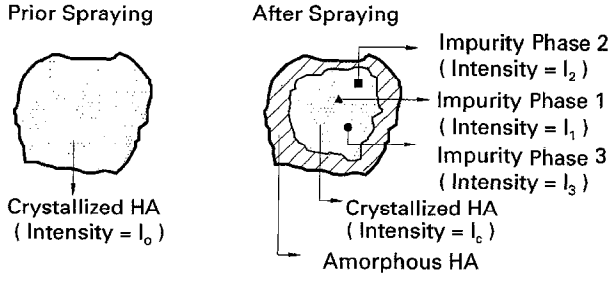

Figure 1 Schematic representation of the determinations of CIP and IOC.

defined as follows (Fig. 1):

$$\text{IOC} = \frac{I_c}{I_0} \times 100\%$$

where I_c is the main peak intensity of HA phase in each HAC. Coatings with higher IOC value yield better degrees of crystallinity.

2.3.3. Microstructure of HACs

The surface morphology of HACs was assessed by scanning electron microscope (SEM, JEOL JSMr 840). Thereafter, the surface roughness R_a) was evaluated (Surfcorder SE-40D, Kosaka Laboratory Ltd.).

3. Results

3.1. Phase composition and crystallinity of HAP and HACs

3.1.1. HAP

As illustrated in Fig. 2a, the XRD pattern revealed that the HAP was a well-crystallized single phase of $Ca_{10}(PO_4)_6(OH)_2$ (JCPDS #9–432).

3.1.2. HACs sprayed by Group I PSPs

In Group I PSPs (Table I), where H_2 gas served as the secondary plasma gas, the influence of PSPs on the phase purity and crystallinity of 27 HACs was evaluated.

The influence of H_2 content. The XRD patterns for three HACs sprayed with different H_2 contents are shown in Fig. 2b–d. By comparing Fig. 2b–d with Fig. 2a, the difference in the phase composition and crystallinity between HACs and HAP can be seen. Apart from HA phase, several impurity phases including α-$Ca_3(PO_4)_2$ (α-TCP), β-$Ca_3(PO_4)_2$ (β-TCP), $Ca_4P_2O_9$ (TP), and CaO were identified in the HACs. Moreover, it was found that the crystallinity of HACs was significantly lower than that of HAP.

The change in phase purity and crystallinity of HACs with H_2 content was evaluated. The concentration of impurity phase (CIP) increased with increasing H_2 content (Fig. 3). With regard to the degree of crystallinity, it is noted that the IOC values decreased with increasing H_2 content (Fig. 4a). These findings indicate that the increase in H_2 content has an adverse effect on phase purity and crystallinity.

The influence of spraying current (SA). Fig. 5 shows the XRD patterns of HACs prepared using different SA. The HACs still contained impurity phases and less crystallinity. The CIP values increased with an increase in SA (Fig. 6), but the IOC values decreased with increasing SA (Fig. 7a). The SA variable revealed the same effect on CIP and IOC as did the H_2 content.

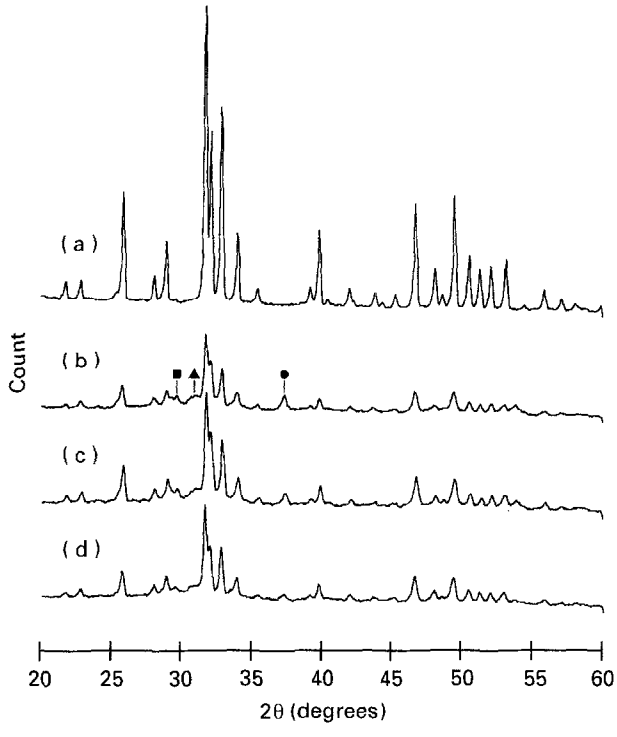

Figure 2 XRD patterns of: (a) HAP revealing single phase of $Ca_{10}(PO_4)_6(OH)_2$; (b) HAC sprayed with H_2 at 10 l/min; (c) HAC sprayed with H_2 at 6 l/min; and (d) HAC sprayed with H_2 at 2 l/min (SA = 600 A and SOD = 7.5 cm). ▲ α,β-$Ca_3(PO_4)_2$(TCP); ■ $Ca_4P_2O_9$(TP); ● CaO.

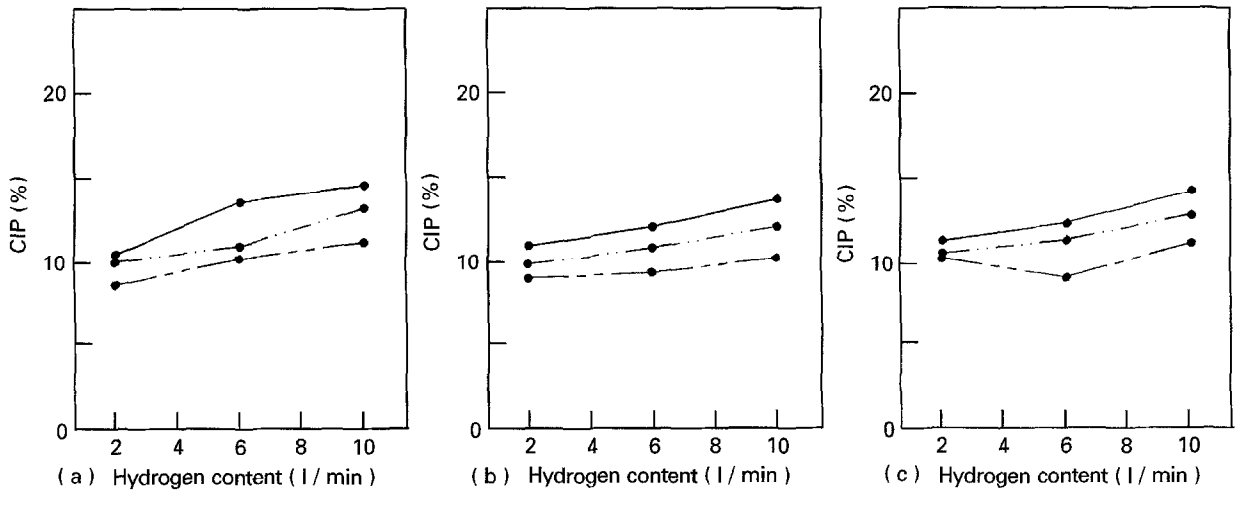

Figure 3 The variation of CIP values of Group I HACs with H_2 content: (a) SOD = 7.5 cm; (b) SOD = 15 cm; (c) SOD = 22.5 cm. —— SA = 600 A; – · · – SA = 500 A; – – – – SA = 400 A.

The influence of stand-off distance (SOD). By altering SOD, the HACs exhibited impurity phases and less crystallinity, as illustrated by the XRD patterns (Fig. 8). The changes in the SOD, being different from the effects of H_2 content and SA, showed little influence on CIP values of HACs (Fig. 9). Nevertheless, the SOD variable did affect IOC values of HACs (Fig. 7b): IOC values decreased with increasing SOD. This means that the coating crystallinity was reduced as SOD was increased.

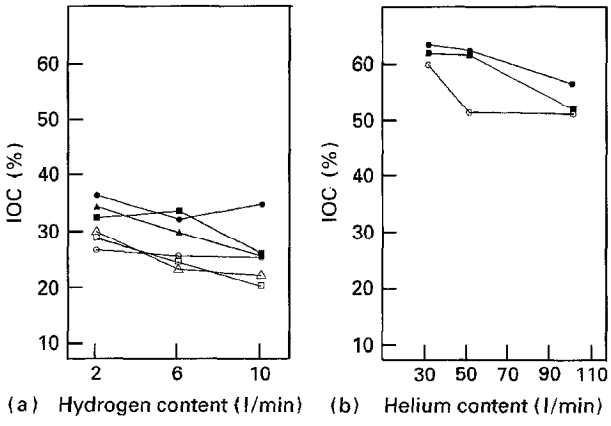

Figure 4 The influence of (a) H_2 content and (b) He content and other PSPs on IOC values. It is noted that IOC values higher than 50% were obtained for Group II HACs. (a) SA; SOD = ■ 600 A; 7.5 cm, △ 600 A; 15 cm, □ 600 A; 22.5 cm, ● 400 A; 7.5 cm, ▲ 400 A; 15 cm, ○ 400 A; 22.5 cm. (b) SA; SOD = ■ 600 A; 7.5 cm, ○ 500 A, 7.5 cm, ● 400 A; 7.5 cm.

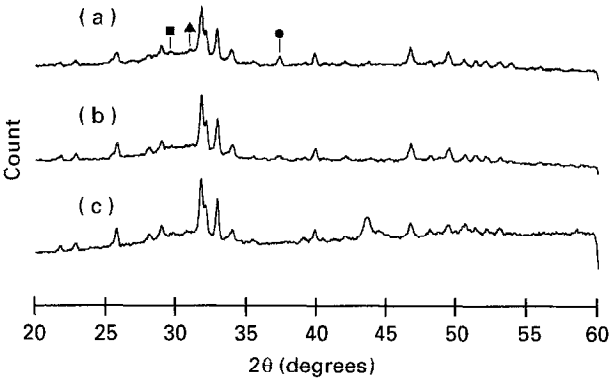

Figure 5 XRD patterns of Group I HACs sprayed at (a) SA = 600 A; (b) SA = 500 A; and (c) SA = 400 A, with H_2 at 10 l/min and SOD = 22.5 cm. ▲ α,β-$Ca_3(PO_4)_2$(TCP); ■ $Ca_4P_2O_9$(TP); ● CaO.

3.1.3. HACs sprayed by Group II PSPs

In Group II PSPs (Table I), where He gas was used as the secondary plasma gas, the influence of PSPs on the phase purity and crystallinity of further 27 HACs was assessed.

The influence of He content and spraying current (SA). The XRD patterns of three HACs sprayed using different He contents are shown in Fig. 10. The phase composition and crystallinity of Group II HACs differed from those of Group I HACs (Figs 2, 5, and 8). The impurity phases almost disappeared and the crystallinity increased significantly.

CIP values increased with increasing He content and increasing SA (Fig. 11). However, it is worth noting that the Group II HACs consisted of almost 95% HA phase (CIP < 5%). Moreover, the IOC value of Group II HACs (Fig. 4b) was significantly higher than that of Group I HACs (Fig. 4a). HACs with IOC value higher than 50% were obtained, although IOC values decreased with increasing He content and SA (Fig. 4b). The highest HAC crystallinity (IOC = 63.5%) was observed when PSPs of He = 30 l/min, SA = 400 A and SOD = 7.5 cm were employed. Group II HACs displayed better results in terms of phase purity and degree of crystallinity.

The influence of stand-off distance (SOD). When the SOD was enlarged from 7.5 cm to 15 cm or 22.5 cm, the deposition efficiency of coating decreased significantly. This suggests that almost no HAC was formed on the Ti–6Al–4V substrate, and that such PSPs (He gas combined with large SOD) are not suitable and should not be used for HAC.

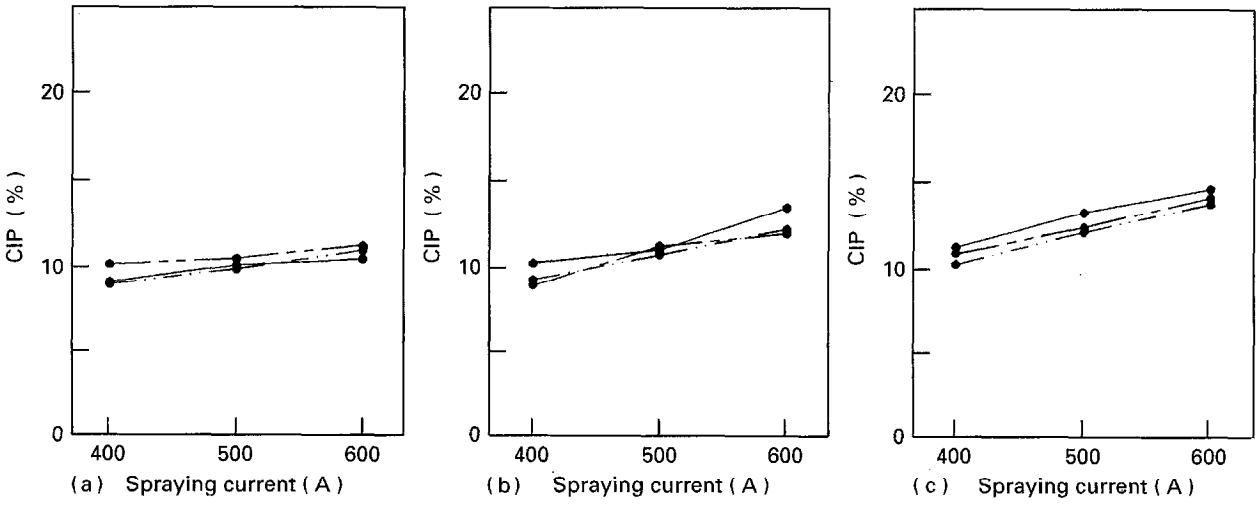

Figure 6 The variation in CIP values of Group I HACs with SA: H_2 = (a) 2 l/min; (b) 6 l/min; (c) 10 l/min. SOD = —— 7.5 cm; – · · – 15 cm; – – – 22.5 cm.

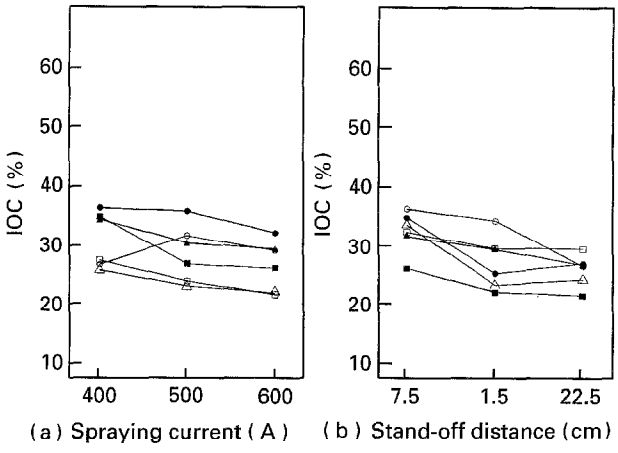

Figure 7 Variation in IOC values with increasing SA (a) and SOD (b). (a) H_2; SOD = ■ 10 l/min; 7.5 cm, △ 10 l/min; 15 cm, □ 10 l/min; 22.5 cm, ● 2 l/min, 7.5 cm, ▲ 2 l/min; 15 cm, ○ 2 l/min; 22.5 cm. (b) SA; H_2 = ■ 600 A; 10 l/min, △ 600 A; 6 l/min, □ 600 A; 2 l/min, ● 400 A; 10 l/min, ▲ 400 A; 6 l/min, ○ 400 A; 2 l/min.

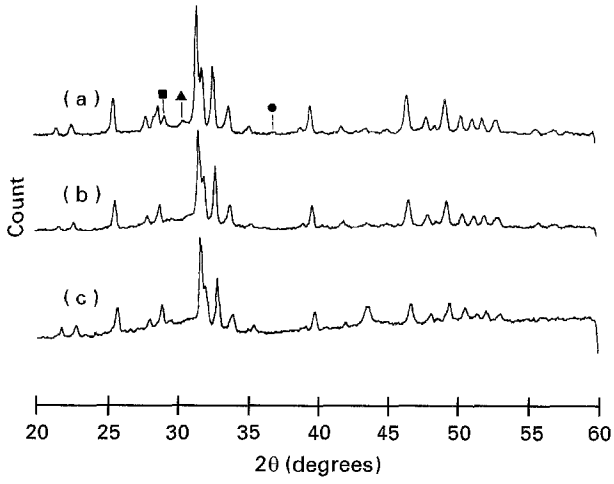

Figure 8 XRD patterns of Group I HACs sprayed at (a) SOD = 7.5 cm; (b) SOD = 15 cm; and (c) SOD = 22.5 cm, with H_2 at 2 l/min and SA = 400 A ▲ α, β-$Ca_3(PO_4)_2$(TCP); ■ $Ca_4P_2O_9$(TP); ● CaO.

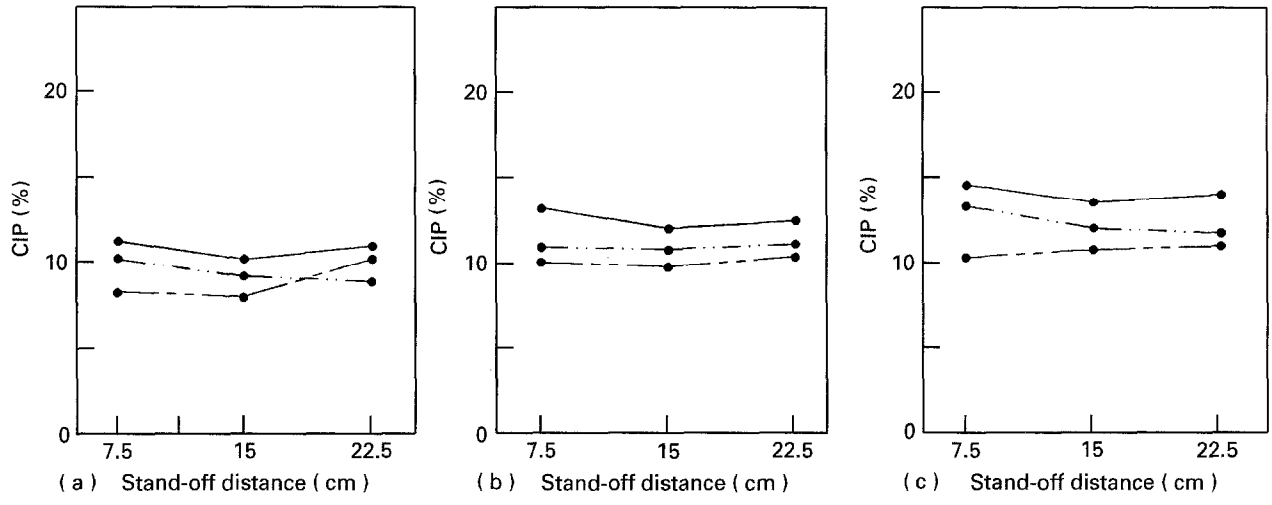

Figure 9 Variation in CIP values of Group I HACs with SOD: (a) SA = 400 A; (b) SA = 500 A; (c) SA = 600 A. H_2 = —— 10 l/min; -·-· 6 l/min; - - - - 2 l/min.

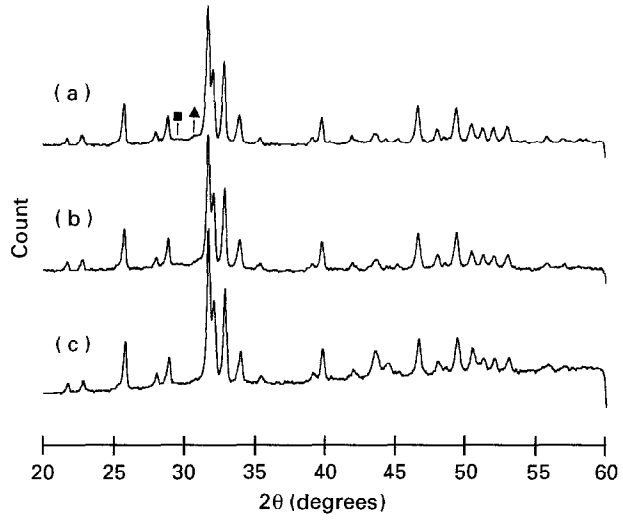

Figure 10 XRD patterns of Group II HACs sprayed at (a) He = 100 l/min; (b) He = 50 l/min; and (c) He = 30 l/min; with SA = 600 A and SOD = 7.5 cm. Group II HACs showed better results in terms of extent of phase purity and degree of crystallinity. ▲ α, β-$Ca_3(PO_4)_2$(TCP); ■ $Ca_4P_2O_9$ (TP)

3.2. Microstructure of HACs

The surface morphology of HACs was assessed by scanning electron microscopy (SEM). The main focus was on the extent of melting that could be observed from the surface area covered by accumulated and/or well-flattened molten splats. Six types of surface morphologies were distinguished and categorized as follows:

Type A1: molten coating consisting of well-flattened and accumulated splats (Fig. 12a, b).

Type A2: molten coating consisting of well-flattened but dispersed (major) and accumulated (minor) splats (Fig. 12c, d).

Type B1: molten coating consisting of re-spheroidized droplets and well-flattened splats (Fig. 12e, f).

Type B2: molten coating with respheroidized but shrunken droplets and dispersed splats (Fig. 12g, h).

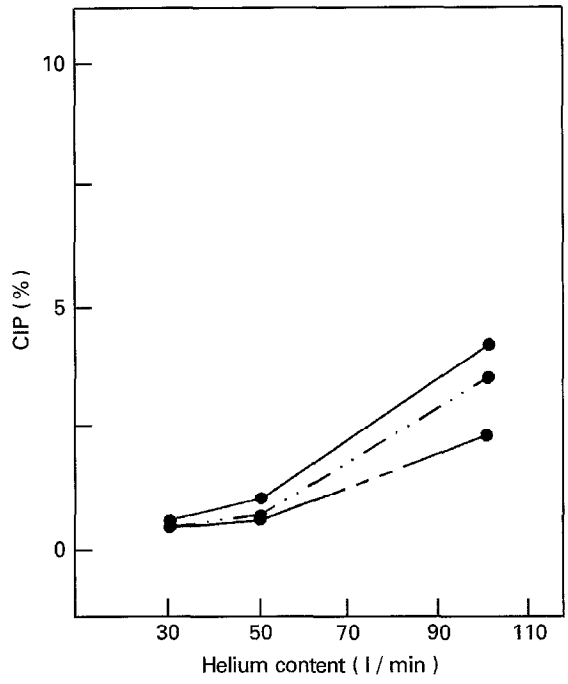

Figure 11 The variation of CIP values of Group II HACs with He content and SA (—— SA = 600 A; –··– SA = 500 A; – – – SA = 400 A). The CIP value was found to be less than 5%.

Figure 12 The surface morphologies of HACs after plasma spraying. The six types include: (a) molten HAC with well-flattened (W) and accumulated (A) splats; (b) higher magnification of (a) showing the 'W' splats; (c) molten HAC with well-flattened but dispersed (WD) and 'A' splats; (d) higher magnification of (c) showing the 'WD' splats; (e) molten HAC with respheroidized (R) droplets and 'W' splats; (f) higher magnification of (e) showing the 'R' droplets; (g) molten HAC with respheroidized but smaller (RS) droplets and 'W' splats; (h) higher magnification of (g) showing the 'RS' droplets; (i) partially molten HAC with unmelted powders (P) and 'W' splats; (j) higher magnification of (i) showing the unmelted 'P' powders; (k) partially molten HAC consisted mostly of the unmelted 'P' powders; (l) higher magnification of (k) showing the unmelted 'P' powders.

Type C1: partially molten coating consisting of unmelting powders and well-flattened splats (Fig. 12i, j).

Type C2: partially molten coating consisting of unmelting powders (major) and flattened splats (minor) (Fig. 12l, m).

The surface roughness (R_a) for each type of surface morphology was examined and is listed in Table III.

Changes in PSPs influenced the surface morphology and roughness. In Group I PSPs, HACs with high extent of melting and high irregularity were formed when the PSPs contained high H_2 content and

TABLE III Surface roughness (R_a) measurements for six types of morphologies

Type	Roughness, R_a (μm)
A1	14.48 ± 2.10
A2	10.20 ± 1.11
B1	7.65 ± 0.57
B2	6.33 ± 0.78
C1	5.10 ± 0.48
C2	4.46 ± 0.35

Values are given as mean ± SD
Six samples were measured for each type of morphology

SA (Type A1 and A2). However, as the SOD was enlarged, coating irregularity decreased because the respheroidized droplets had become a major part of the surface (Type B1 and B2). In Group II PSPs, partially molten coatings (Type C1 and C2), revealing great difference in surface morphology from the molten ones (Type A1, A2, B1 and B2), could be observed. Since the unmelted particles appeared widespread on the coating surface, the surface roughness was minimized.

4. Discussion

The phase composition of plasma-sprayed HACs has been investigated by many researchers. Some reported that the HAC consisted of almost pure HA phase with barely detectable extra phases [19, 23, 26], while others indicated that the HAC contained many impurity phases [14, 22, 27–28]. Differences in the results of phase composition are obvious. This might be attributed to the fact that different PSPs, especially the spraying atmosphere, were employed. However, the plasma atmosphere used in previous studies was commonly not reported. Based on the results of phase identification in this study, the phase composition of HACs was determined to be dominantly influenced by the plasma atmosphere. Specifically, HACs sprayed with H_2 (Group I) revealed a mixture of HA phase with a large amount of α, β-TCP, TP and CaO phase; these impurity phases being consistent with the identifications of Ducheyne *et al.* [14] and Gross *et al.* [22]. In contrast, HACs sprayed with He (Group II) consisted of nearly pure HA phase. This kind of HAC is similar to the HAC obtained by Radin *et al.* [23], who reported that the HAC (HAF-PS coating) consisted of 95% apatite with little extra phases.

The formation mechanisms of impurity phases in HACs have been discussed in [21, 23]. Since plasma spraying subjects the HA material to high temperatures with abundant heat content, phase stability of HA no longer holds and the HA phase tends to decompose. The phase decomposition probably proceeds in several steps: at high temperature, possibly above 1450 °C, there is decomposition of HA to form α-TCP and TP [29, 30]. Being an unstable phase at room temperature, α-TCP naturally transforms to β-TCP (stable phase at room temperature) at about 1100 °C. If the environment involves a high heat content, the TP phase would further decompose to form HA and CaO [29, 30].

From the above discussion, the reasons for the distinctive difference in phase composition between Group I and Group II HACs are clear. Because the heat content of diatomic H_2 gas is higher than that of mono-atomic He gas [31], the higher heat content in the plasma (Group I) provides a greater ability to melt the starting HAP, leading to more opportunities for phase decomposition. As a result, higher values of CIP were obtained for HACs sprayed using Group I PSPs. In the same way, the CIP values increased with H_2 content (Fig. 3) and SA (Fig. 6) owing to increasing heat content in the PSPs. In contrast, high phase purity of Group II HACs, revealing lower CIP values (Fig. 11), is due to lower heat content of the PSPs involved. Since the heat content of the plasma was not changed with variation of SOD, the CIP values of HACs were not influenced by the SOD variable (Fig. 9).

There are several methods proposed to determine quantitatively the concentration of a particular phase in a mixture of phases using the XRD patterns [32]. However, in practice, precise quantitative analysis seems to be difficult because of some complicating factors. For instance, crystal structures, lattice parameters and absorption coefficient of phases all influence the results of quantitative analyses. In this study, we provide a practical method (Fig. 1) which gives a good estimation of impurity phases *in situ*. Through the method of CIP calculation (I_{im}/I_0), the relative concentration of impurity phase can be assessed from the intensity of phases, although the relation between intensity and concentration is not generally linear. Another beneficial effect of this method is that it avoids the complicated effect from the the amorphous component contributed by the impurity phases.

Lower crystallinity, or short-range three-dimensional periodicity of atomic arrangement observed in HACs was another problem related to the plasma spraying process since the HA ceramic was supercooled from high temperature. As one of the requirements suggested in the literature [3], the crystalline structure of HACs should not be altered irreversibly. Nevertheless, irreversible plasma-spraying-induced changes in crystallinity of HACs has been reported [18, 19, 21–23]. In a report by Koch *et al.* [21], the concept of crystallinity of plasma-sprayed HACs was discussed in detail. They found that the crystallite size of HA, defined as the average size of a domain within a powder particle that has a coherently diffracting monocrystalline structure, decreased ten- to 100-fold after spraying. Yet, the degree of crystallinity has not been quantitatively assessed. In this study, to determine the crystallinity quantitatively, the method of IOC calculation was introduced using the starting HAP as a reference standard (I_c/I_0). This method is similar to that proposed in [33, 34].

It is suggested that coating crystallinity is influenced physically by the retaining original crystalline phase and the degree of supercooling. As the retaining original crystalline phase is decreased and/or the degree of supercooling is increased during spraying, coating

crystallinity decreases. Findings in this study revealed that both the spraying atmosphere and the SOD influenced the results of IOC calculations. Since the Group II HACs (He atmosphere) were partially molten (Type C1 and C2 in Fig. 12), the original crystalline HA phase was most probably retained. As a result, the coating crystallinity retained at least 50% (Fig. 4b) of the original HAP crystal structure, and the highest coating crystallinity (IOC = 63.45%) was obtained. On the opposite end, less coating crystallinity was found for Group I HACs (H_2 atmosphere) not only because they contained little retaining original crystalline phase (HAP has been melted completely), but also because they were subject to a high degree of supercooling as they were sprayed (higher heat content would result in a higher degree of supercooling). Moreover, the IOC value of Group I HACs decreased with an increase in SOD (Fig. 7b). As the SOD was increased, the temperature of the metal substrate was lowered, resulting in an increase of supercooling. The lowest crystallinity (IOC = 21.9%) (arrow in Fig. 7b) was obtained for one of the Group I HACs sprayed with the highest H_2 content and largest SOD.

Surface morphologies and related roughness of HACs have been evaluated by many researchers [9, 21–23]. In the study by Gross *et al.* [22], HACs with cracked, partially molten, good splat formation, and respheroidized droplets surface were observed, coincident with our findings. A later report also obtained an HAC crack-free surface [24]. However, high magnification photographs did not reveal the overall features of the coating. Therefore, investigation of HAC microstructure at lower magnification is needed. In this study, the systematic relationship between PSPs and microstructure was assessed.

With the aid of SEM observations at lower magnification, changes in plasma atmosphere, resulting in different heat content, were found to be the primary influence on surface morphology and roughness. HACs sprayed using a H_2 atmosphere (more heat content) revealed molten and rougher morphologies (Type A1, A2, B1 and B2) because the feedstock HAP was melted completely. In contrast, HACs sprayed using a He atmosphere (less heat content) exhibited partially molten and smooth morphologies (Type C1 and C2) owing to the fact that the heat content was insufficient to melt the feedstock HAP completely. The SOD variable in Group I PSPs also affected the results of roughness measurements. The coating irregularity underwent a significant decrease as the SOD was increased. The reason was that the respheroidized droplets had become a major part of the surface.

Surface characteristics of implants might influence bone integration and, consequently, lead to differences in the interfacial strength of bone–implant contact. In a study by Buser *et al.* [9], the extent of cancellous bone–Ti implant interface was demonstrated to be positively correlated with increased roughness of the implant surface. Moreover, Steinemann *et al.* [35] found that the removal torque for titanium plasma-sprayed (TPS) implants was higher than that for smooth implants. Therefore, the increase in surface roughness of HA plasma-sprayed implants (Group I HACs) might be beneficial to bone apposition and biomechanical strength. However, this statement needs to be further evaluated.

Owing to either the appearance of impurity phases or the phenomenon of lower crystallinity in HACs, the biological responses of HACs are of some concern. Though TCP and TP phases were reported to be biocompatible [36–38], the resolvability of TCP phase and the hydrolyzation of TP phase would leave a porous coating and thereby decrease the mechanical strength of the coating. Since the CaO phase had no biocompatibility, it was considered to be the most detrimental phase following implantation. The amorphous component in the coating was undesirable since it was rapidly resorbed [9]. As a consequence, Group II HACs with high phase purity and crystallinity were favoured for biological applications. However, it should be noted that there is a conflict between surface morphology, phase purity and crystallinity. Clinically, to provide long-term implant fixation, the bonding strength between HAC and metallic substrate is required to be as high as possible. Based on this point, application of partially molten Group II HACs having potentially, a weak bonding is thereby limited. On the other hand, molten Group I HACs having potentially strong bonding might provide long-term fixation, though they contain higher impurity phases and have lower crystallinity. Thus characteristics such as bonding strength and dissolution rate of HACs should be further evaluated [39].

As suggested by Geesink [16], characteristics affecting the ultimate behaviour of an HAC include: (1) coating thickness; (2) mechanical strength of the coating; (3) porosity of the coating; (4) chemical purity of HA after spraying; (5) crystallinity of the HA material; and (6) dissolution properties of the coating. These items determine the biological longevity of the coating and thereby influence the clinical outcome [2]. Some general guidelines have been given. A thin coating of about 50–70 μm with full-density was demonstrated to give high bonding strength with the substrate [1, 4, 5, 25], and to overcome resorption [5, 40]. However, optimum values for chemical purity and crystallinity have not yet been established. Although an HA content of over 95% and HA crystallinity over 70% after spraying were proposed [16], the exact quantitative method used was not clear. In this study, we have provided quantitative analyses to determine relatively the phase concentration and crystallinity of HACs. Based on the results of CIP and IOC calculations, different biological responses related to the phase concentration and crystallinity of HACs can be further evaluated *in vitro* and *in vivo* [39].

5. Conclusions

The relationships between PSPs and coating characteristics were systematically evaluated. To determine quantitatively the extent of phase purity and degree of crystallinity of HACs, the terms CIP and IOC were introduced, respectively. The conclusions of this study

are summarized as follows.

(1) Coating characteristics including phase purity, crystallinity, morphology and roughness were affected by the PSPs, especially the spraying atmosphere. Group I HACs (H_2 atmosphere) contained higher impurity phases (higher CIP values), less crystallinity (lower IOC values) and better melting of the coating. In contrast, Group II HACs (He atmosphere) revealed lower impurity levels (lower CIP values), higher crystallinity (higher IOC values) and worse melting of the coating.

(2) The CIP values of Group I HACs increased with H_2 content and SA, but were not related to the SOD.

(3) The IOC values of Group I HACs decreased with increasing H_2 content, SA and SOD.

(4) Coatings with a better extent of melting revealed higher irregularity.

(5) Coatings (Group II HACs) consisting of at least 50% (IOC > 50%) of the original crystalline structure and almostly 95% (CIP < 5%) apatite with barely detectable extra phases were obtained.

(6) It should be noted that the achievement of both better melting of the coating (Group I HACs) and higher phase purity (Group II HACs) is difficult.

(7) Based on the results of this study, HACs with specified coating characteristics could be obtained and, consequently, biological responses related to different coating characteristics can be further evaluated *in vitro* and *in vivo*.

Acknowledgements

The authors thank T. M. Lee and M. L. Tsai for their technical assistance in the specimen fabrications. This study was supported in part by grant MOEA 38S4140 from the Industrial Technology Research Institute, Hsinchu, Taiwan.

References

1. K. DE GROOT, R. GEESINK, C. P. A. KLEIN and P. SEREKIAN, *J. Biomed. Mater. Res.* **21** (1988) 1375.
2. J. E. LEMONS, *Clin. Orthop.* **235** (1988) 220.
3. W. R. LACEFIELD, in "Bioceramics: material characteristics versus in vivo behavior", edited by P. Ducheyne and J. E. Lemons, *Ann. N. Y. Acad. Sci.* **523** (1988) 72.
4. E. MUNTING, M. VERHELPEN, F. LI and A. VINCENT, in "CRC handbook of bioactive ceramics", edited by T. Yamamuro, L. L. Hench and J. Wilson (CRC Press, Boca Raton, MA, 1990) pp. 143–148.
5. R. G. T. GEESINK, K. DE GROOT and P. A. K. T. CHRISTEL, *Clin. Orthop.* **225** (1987) 147.
6. R. G. T. GEESINK, K. DE GROOT and C. P. A. T. KLEIN, *J. Bone Joint Surg.* **70B** (1988) 17.
7. H. W. DENISSEN, W. KALK, H. M. de NIEUPORT, J. C. MALTHA and A. VAN DE HOOFF, *Int. J. Prosth.* **3** (1990) 53.
8. K. HAYASHI, K. UENOYAMA, N. MASUGUCHI and Y. SUGIOKA, *J. Biomed. Mater. Res.* **25** (1991) 515.
9. D. BUSER, R. K. SCHENK, S. STEINEMANN, J. P. FIORELLINI, C. H. FOX and H. STICH, *ibid.* **25** (1991) 889.
10. J. A. JANSEN, J. P. C. M. VAN DE WAERDEN, J. G. C. WOLKE and K. DE GROOT, *ibid.* **25** (1991) 973.
11. M. GOTTLANDER and T. ALBREKTSSON, *Int. J. Oral Maxillofac. Imp.* **6** (1991) 339.
12. B. C. WANG, E. CHANG, D. TU and C. Y. YANG, *J. Mater. Sci.: Mater. Med.* **4** (1993) 394.
13. S. D. COOK, K. A. THOMAS, J. F. KAY and M. JARCHO, *Clin. Orthop.* **230** (1988) 303.
14. P. DUCHEYNE, J. CUCKLER, S. RADIN and E. NAZAR, in "CRC handbook of bioactive ceramics", edited by T. Yamamuro, L. L. Hench and J. Wilson (CRC Press, Boca Raton, MA, 1990) pp. 123–131.
15. P. DUCHEYNE and K. E. HEALY, *J. Biomed. Mater. Res.* **22** (1988) 1137.
16. R. G. T. GEESINK, *Clin. Orthop.* **261** (1990) 39.
17. T. W. BAUER, R. G. T. GEESINK, R. ZIMMERMAN and J. T. MCMAHON, *J. Bone Joint Surg.* **73A** (1991) 1439–1452.
18. J. F. KAY, in "CRC handbook of bioactive ceramics", edited by T. Yamamuro, L. L. Hench and J. Wilson (CRC Press, Boca Raton, MA, 1990) pp. 111–122.
19. K. DE GROOT, C. P. A. T. KLEIN, J. G. C. WOLKE and J. M. A. DE BLIECK-HOGERVORST, in *ibid.* pp. 133–142.
20. C. P. A. T. KLEIN, P. PATKS, H. B. M. VAN DER LUBBE, J. G. C. WOLKE and K. DE GROOT, *J. Biomed. Mater. Res.* **25** (1991) 53.
21. B. KOCH, J. G. C. WOLKE and K. DE GROOT, *ibid.* **24** (1990) 655.
22. K. A. GROSS and C. C. BERNDT, in 2nd Plasma-Technik-Symposium, Lucerne, Switzerland, June 5th to 7th, **3** (1991) 159.
23. S. R. RADIN and P. DUCHEYNE, *J. Mater. Sci.: Mater. Med.* **3** (1992) 33.
24. D. M. LIU, Z. C. LOU and H. M. CHOU, 19th Annual Meeting of the Society for Biomaterials in conjunction with the 25th International Biomaterials Symposium, April 28-May 2, 1993.
25. B. C. WANG, E. CHANG, C. Y. YANG, D. TU and C. H. TSAI, *Surf. Coat. Technol.* **58** (1993) 107.
26. M. J. FILIAGGI, N. A. COOMBS, R. M. PILLIAR, *J. Biomed. Mater. Res.* **25** (1991) 1211.
27. HUAXIA JI, C. B. PONTON, P. M. MARQUIS, *J. Mater. Sci: Mater Med.* **3** (1992) 283–287.
28. HUAXIA JI, P. M. MARQUIS, *Biomaterials* **14** (1993) 64–68.
29. American Ceramic Society, "Phase diagrams for ceramicists", Vol 5 American Ceramic Society, Washington, DC, 1983). p. 320.
30. K. de GROOT, C. P. A. T. KLEIN, J. G. C. WOLKE, and J. M. A. de BLIECK-HOGERVORST, in "CRC handbook of bioactive ceramics", edited by T. Yamamuro, L. L. Hench and J. Wilson (CRC Press, Boca Raton, MA, 1990) pp. 3–16.
31. H. S. INGHAM and A. P. SHEPHARD (eds), "Flame spray handbook", 1st Edn (METCO Inc., Long Island, New York, 1965) p. 11.
32. B. D. CULLITY (ed.), "Elements of X-ray diffraction", 2nd Edn (Addison-Wesley, New York, 1978) pp. 409–417.
33. E. P. BUTLER, *Acta Metall.* **18** (1970) 347.
34. P. C. CLAPP and S. C. MOSS, *Phys. Rev.* **171** (1971) 764.
35. S. G. STEINEMANN, J. EULENBERGER, P. A. MAUSLI and A. SCHROEDER, in "Advances in biomaterials", edited by P. Christel, A. Meunier and A. J. C. Lee, (Elsevier Science Publishers B. V., Amsterdam, 1986) pp. 409–414.
36. K. SHIMAZAKI and V. MOONEY, *J. Orthop. Res.* **3** (1985) 301.
37. P. S. RGGLI, W. MULLER and R. K. SCHENK, *Clin. Orthop.* **232** (1988) 127.
38. L. XIE and E. A. MONROE, in "CRC handbook of bioactive ceramics", edited by T. Yamamuro, L. L. Hench and J. Wilson (CRC Press, Boca Raton, MA 1990) pp. 29–37.
39. C. Y. YANG, B. C. WANG, E. CHANG and B. C. WU, *J. Mater. Sci: Mater. Med.* **6** (1995) 258.
40. C. P. A. T. KLEIN, A. A. DRIESSEN and K. DE GROOT, *Biomaterials* **5** (1984) 157.

Received 7 June 1993
and accepted 13 May 1994